International Journal of Nanomedicine

Dovepress
open access to scientific and medical research

Open Access Full Text Article

ORIGINAL RESEARCH

RGDV-modified gemcitabine: a nano-medicine capable of prolonging half-life, overcoming resistance and eliminating bone marrow toxicity of gemcitabine

This article was published in the following Dove Press journal:
International Journal of Nanomedicine

Wenchao Liu[1,2]
Yujia Mao[1,2]
Xiaoyi Zhang[1,2]
Yaonan Wang[1,2]
Jianhui Wu[1,2]
Shurui Zhao[1,2]
Shiqi Peng[1,2]
Ming Zhao[1–3]

[1]Beijing Area Major Laboratory of Peptide and Small Molecular Drugs, Department of Medicinal Chemistry, School of Pharmaceutical Sciences, Capital Medical University, Beijing 100069, People's Republic of China; [2]Engineering Research Center of Endogenous Prophylactic of Ministry of Education of China, Department of Medicinal Chemistry, School of Pharmaceutical Sciences, Capital Medical University, Beijing 100069, People's Republic of China; [3]Department of Biomaterials, Beijing Laboratory of Biomedical Materials and Key Laboratory of Biomedical Materials of Natural Macromolecules, Beijing University of Chemical Technology, Beijing 100026, People's Republic of China

Correspondence: Ming Zhao
Beijing Area Major Laboratory of Peptide and Small Molecular Drugs, Department of Medicinal Chemistry, School of Pharmaceutical Sciences, Capital Medical University, No. 10, Youanmenwaixitoutiao, Fengtai District, Beijing 100069, People's Republic of China
Tel +86 108 391 1535
Email mingzhao@bjmu.edu.cn

Background: Gemcitabine has been widely used as a chemotherapeutic drug. However, drug resistance, short half-life and side effects seriously decrease its chemotherapeutic efficacy.

Purpose: The object of preparing RGDV-gemcitabine was to prolong the half-life, to overcome drug resistance and to eliminate bone marrow toxicity of gemcitabine.

Methods: Arg-Gly-Asp-Val was coupled with gemcitabine, forming 4-(Arg-Gly-Asp-Val-amino)-1-[3,3-difluoro-4-hydroxy-5-(hydroxylmethyl)oxo-lan-2-yl]pyrimidin-2-one (RGDV-gemcitabine) involving 9-step reactions. The advantages of RGDV-gemcitabine to gemcitabine were demonstrated by a series of assays, such as in vitro half-life assay, in vitro drug resistance assay, in vivo anti-tumor assay, in vivo kidney toxicity assay, in vivo liver toxicity assay and in vivo marrow toxicity assay. The nano-features of RGDV-gemcitabine were visualized by TEM, SEM and AFM images. The tumor-targeting action and release of RGDV-gemcitabine were evidenced by FT-MS spectra.

Results: Half-life and anti-tumor activity of RGDV-gemcitabine were 17-fold longer and 10-fold higher than that of gemcitabine, respectively. RGDV-gemcitabine, but not gemcitabine, showed no kidney toxicity, no liver toxicity, no marrow toxicity and no drug resistance. The advantages attributed to the nanofeatures of RGDV-gemcitabine were targeting tumor tissue and releasing gemcitabine in tumor tissue.

Conclusion: RGDV-gemcitabine successively overcame the defects of gemcitabine and provided a practical strategy of nano-medicine.

Keywords: gemcitabine, modification, half-life, anti-tumor, tumor targeting, release, toxicity, nano-species

Introduction

Gemcitabine has been used as a chemotherapeutic drug over 20 years, and it is a standard treatment choice for the locally advanced cancer, metastatic pancreatic cancer, breast cancer and ovarian cancer.[1–6] The combinations of gemcitabine with the other drugs including oxaliplatin, irinotecan, miR-345, nab-paclitaxel, RT11-i antibody, metformin, ginkgolide B and melatonin are approved been able to enhance the efficacy of gemcitabine in the treatment of pancreatic cancer.[7–13] Thus the combination of gemcitabine with platinum, carboplatin, sorafenib, paclitaxel, cisplatin plus bevacizumab and docetaxel is used for bladder cancer and muscle-invasive bladder cancer,[7,14]

submit your manuscript | www.dovepress.com
DovePress
http://doi.org/10.2147/IJN.S212978

advanced breast cancer,[15] germ cell cancer,[16] metastatic or unresectable transitional-cell carcinoma,[17] recurrent urothelial carcinoma of bladder,[18] concomitant primary lung cancer and metastatic pulmonary colorectal cancer[19] and soft tissue sarcomas,[20] respectively.

Gemcitabine is used to increase indications when combining with other agents. Thus the combination of gemcitabine with licoricidin, taxanes, triptolide, chlorambucil and lentinan is used for osteosarcoma,[21] advanced or metastatic urothelial cancer,[22] bladder cancer,[23] hepatocellular carcinoma[24] and the urothelial bladder cancer,[25] respectively. Therefore, either as the first-line chemotherapeutic drug or as one member of the second-line chemotherapeutic regimen, gemcitabine is widely valued.

On the other hand, in the past 20 years, drug resistance,[1–6] short half-life[26] and side effects[27,28] seriously decrease the chemotherapeutic efficacy of gemcitabine. To overcome these shortcomings, the efforts are focused on the development of the micelles, the liposomes and g-quadruplex aptamer of gemcitabine.[29–39]

To increase the chemotherapeutic efficacy of gemcitabine, this investigation was started from the design of a reasonable lead compound of having long half-life. In this regard, tetrahydroisoquinoline-3-carboxyl-Ile-gemcitabine, Asp(OBzl)-gemcitabine and 4-(Arg-Gly-Asp-Val-amino)-1-[3,3-difluoro-4-hydroxy-5-(hydroxylmethyl)oxo-lan-2-yl]pyrimidin-2-one (RGDV-gemcitabine) were prepared as 3 candidates to test their in vitro half-life. Figure 1 indicates that in mouse plasma the half-life of these candidates is 3–17 fold longer than that of gemcitabine, and RGDV-gemcitabine has the longest half-life. Thus, RGDV-gemcitabine was selected as a reasonable lead to receive the assays and tests, such as in vitro drug resistance assay, in vivo anti-tumor assay, in vivo kidney toxicity assay, in vivo liver toxicity assay, in vivo marrow toxicity assay, nano-feature test, tumor-targeting test and targeting release test.

Materials and methods

Reagents and instruments

Gemcitabine (J&K Scientific), amino acids (Shang Hai Jier Shenghua), reagents and solvents (Sinopharm Chemical Reagent Co., Ltd) for this work were obtained commercially and used without further purification, unless otherwise specified. TLC and chromatography were performed with Qingdao silica gel GF254 and H60 (Qingdao Haiyang Chemical Co. Ltd, China), respectively. ^{1}H (300 and 800 M Hz) and ^{13}C (75 and 200 MHz) NMR spectra were recorded on Bruker AMX-300 and AMX-800

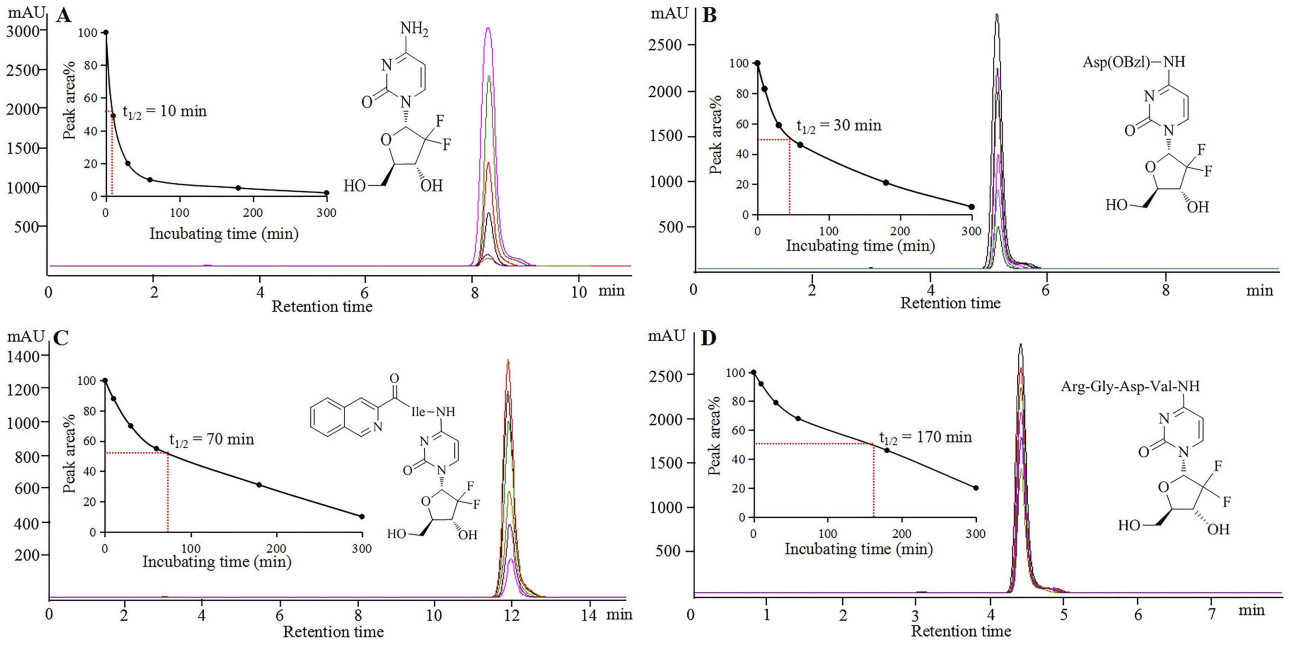

Figure 1 HPLC-UV chromatogram, peak area and half-life. (**A**) After 300 mins incubation, the HPLC-UV chromatogram, peak area and half-life of gemcitabine; (**B**) After 300 mins incubation in mouse plasma, the HPLC-UV chromatogram, peak area and half-life of Asp(OBzl)-gemcitabine; (**C**) After 300 mins incubation, the HPLC-UV chromatogram, peak area and half-life of 1,2,3,4-tetrahydroisoquinoline-3-carboxyl-Ile-gemcitabine; (**D**) After 300 mins incubation, the HPLC-UV chromatogram, peak area and half-life of RGDV-gemcitabine.

Abbreviations: RGDV-gemcitabine, 4-(Arg-Gly-Asp-Val-amino)-1-[3,3-difluoro-4-hydroxy-5-(hydroxylmethyl)oxo- lan-2-yl]pyrimidin-2-one.

spectrometer, while DMSO-d6 and TMS (Sigma) were used as the solvent and the internal standard, respectively. Electrospray ionization mass spectra (ESI-MS) were recorded on a ZQ 2000 mass spectrometer (Waters, USA) or a 9.4 T SolariX Fourier transform ion cyclotron resonance (FT-ICR) mass spectrometer (Bruker, USA) with ESI/matrix-assisted laser desorption/ionization (MALDI) dual ion source. The purity of the compounds was determined by high-performance liquid chromatography (HPLC). HPLC was conducted on an Agilent Technologies 1200 Series HPLC system (Agilent Technologies, Santa Clara, CA, USA) by using Eclipse XDB C18 column (5 μm, 4.6 mm ×150 mm). The column temperature was 40°C. The compounds were eluted with methanol/H_2O. The gradient consisted of 60% methanol (0–5 mins), 70% methanol (5–10 mins), 80% methanol (10–20 mins) and 90% methanol (20–30 mins). The flow rate was 0.8 mL/min.

Animals and cell lines

Male ICR mice (22±2 g) were purchased from the Laboratory Animal Center of Capital Medical University. All evaluations were based on the protocol. The protocol was reviewed and approved by Ethics Committee of Capital Medical University. The committee assured that the animal welfare was maintained in accordance with the requirements of Animal Welfare Act and NIH Guide for Care and Use of Laboratory Animals. Statistical analyses of all biological data were carried out by use of one-way ANOVA. All analyses were done with SPSS 19.0 program and *P*-value <0.05 was considered statistically significant. Human breast cancer (MCF-7), human colorectal carcinoma (HCT-8), human liver hepatocellular (HepG2), human non-small cell lung cancer (A549) and human high metastasis lung cancer (95D) cell lines were purchased from keyGEN BioTECH (Nanjing China).

Synthesis

Boc-Arg(NO_2)-Gly-OBzl

At 0°C, into a solution of 3.19 g (10 mmol) Boc-Arg(NO_2)-OH in 100 mL of anhydrous tetrahydrofuran (THF), 1.35 g (10 mmol) of N-hydroxybenzotriazole (HOBt) and 2.47 g (12 mmol) of dicyclohexylcarbodiimide (DCC) were added, stirred for 30 mins and then 4.04 g (12 mmol) of Tos·H-Gly-OBzl was added. This reaction mixture was at 0°C adjusted to pH 9 with N-methylmorpholine (NMM), at room temperature for 10 hrs and TLC (CH_2Cl_2/CH_3OH, 15/1) indicated the reaction of Boc-Arg(NO_2)-OH and Tos·H-Gly-OBzl been completed. The reaction mixture was filtered, the filtrate was concentrated in vacuum and the residue was dissolved with 150 mL of ethyl acetate. The solution was successively washed with aqueous $NaHCO_3$ (5%, 100 mL ×3), aqueous $KHSO_4$ (5%, 100 mL ×3), aqueous NaCl (26%, 100 mL ×3), aqueous $NaHCO_3$ (5%, 100 mL ×3) and aqueous NaCl (26%, 100 mL ×3). The solution was dried with anhydrous Na_2SO_4 for 12 hrs, filtered, the filtrate was concentrated in vacuum and the residue was purified with silica gel column (CH_2Cl_2/CH_3OH, 35/1) to provide 4.0 g (86%) of the title compound as colorless powders. ESI-MS (m/z): 467 $[M + H]^+$; ^1H NMR and ^{13}C NMR are shown in the Supporting Information.

Boc-Arg(NO_2)-Gly-OH

At 0°C, a solution of 4.0 g (8.58 mmol) of Boc-Arg(NO_2)-Gly-OBzl, 30 mL of CH_3OH and 1 mL of aqueous NaOH (2 M) was stirred for 4 hrs and TLC (CH_2Cl_2/CH_3OH, 15/1) indicated the complete disappearance of Boc-Arg(NO_2)-Gly-OBzl. At 0°C, the reaction mixture was acidified with hydrochloric acid (2 M), evaporated in vacuum and the residue was extracted with ethyl acetate (100 mL ×3). The ethyl acetate phase was dried with anhydrous Na_2SO_4 for 12 hrs, filtered and the filtrate was evaporated in vacuum to provide 2.81 g (88%) of the title compound as colorless powders. ESI-MS (m/z): 375 $[M - H]^-$; ^1H NMR and ^{13}C NMR are shown in the Supporting Information.

Boc-Arg(NO_2)-Gly-Asp(OtBu)-OMe

At 0°C into a solution of 2.81 g (7.47 mmol) of Boc-Arg(NO_2)-Gly-OH in 50 mL of anhydrous THF, 1.01 g (7.47 mmol) of HOBt and 1.85 g (8.96 mmol) of DCC were added, stirred for 30 mins and then 2.15 g (8.96 mmol) of HCl·H-Asp(OtBu)-OMe was added. This reaction mixture was at 0°C, adjusted to pH 9 with NMM, stirred at room temperature for 10 hrs and TLC (CH_2Cl_2/CH_3OH, 15/1) indicated the reaction of Boc-Arg(NO_2)-OH and Tos·H-Gly-OBzl been completed. The reaction mixture was filtered, the filtrate was evaporated in vacuum and the residue was dissolved in 150 mL of ethyl acetate. The solution was successively washed with aqueous $NaHCO_3$ (5%, 100 mL ×3), aqueous $KHSO_4$ (5%, 100 mL ×3), aqueous NaCl (26%, 100 mL ×3), aqueous $NaHCO_3$ (5%, 100 mL ×3) and aqueous NaCl (26%, 100 mL ×3). The solution was dried with anhydrous Na_2SO_4 for 12 hrs, filtered, the filtrate was evaporated in vacuum and the residue was purified with silica gel column (Cl_2CH_2/CH_3OH, 35/1) to provide 3.15 g (75%) of the title compound

as colorless powders. ESI-MS (m/z): 562 $[M + H]^{+;}$ ^{1}H NMR and ^{13}C NMR are shown in the Supporting Information.

Boc-Arg(NO_2)-Gly-Asp(OtBu)-OH

At 0°C, a solution of 3.15 g (5.6 mmol) of Boc-Arg(NO_2)-Gly-Asp(OtBu)-OMe, 30 mL of CH_3OH and 1 mL of aqueous NaOH (2 M) was stirred for 4 hrs and TLC (CH_2Cl_2/CH_3OH, 15/1) indicated the complete disappearance of Boc-Arg(NO_2)-Gly-Asp(OtBu)-OMe. At 0°C, the reaction mixture was acidified with hydrochloric acid (2 M), evaporated in vacuum and the residue was extracted with ethyl acetate (100 mL ×3). The ethyl acetate phase was dried with anhydrous Na_2SO_4 for 12 hrs, filtered and the filtrate was evaporated in vacuum to provide 2.55 g (83%) of the title compound as colorless powders. ESI-MS (m/z): 546 $[M - H]^{-;}$ ^{1}H NMR and ^{13}C NMR are shown in the Supporting Information.

Boc-Arg-Gly-Asp(OtBu)-OH

At room temperature, a suspension of 2.55 g (4.65 mmol) of Boc-Arg(NO_2)-Gly-Asp(OtBu)-OH, 30 mL of CH_3OH and 500 mg of Pd/C was treated with H_2. Then, 12 hrs after the hydrogenolysis, TLC (CH_2Cl_2/CH_3OH, 15/1) indicated the complete disappearance of Boc-Arg(NO_2)-Gly-Asp(OtBu)-OH. The reaction mixture was filtrated and the filtrate was evaporated in vacuum to provide 2.15 g (92%) of the title compound as colorless powders. ESI-MS (m/z): 503 $[M + H]^{+;}$ ^{1}H NMR and ^{13}C NMR are shown in the Supporting Information.

4-Boc-Val-amino-1-[3,3-difluoro-4-hydroxy-5-(hydroxylmethyl)oxolan-2-yl]pyri-midin-2-one (1)

At 0°C into a solution of 2.17 g (10 mmol) of Boc-Val-OH in 100 mL of anhydrous N,N-dimethylformamide (DMF), 1.35 g (10 mmol) of HOBt and 2.47 g (12 mmol) of DCC were added, stirred for 30 mins and then 2.63 g (10 mmol) of gemcitabine was added. This reaction mixture was at 0°C adjusted to pH 9 with NMM, stirred at room temperature for 10 hrs and TLC (CH_2Cl_2/CH_3OH, 10/1) indicated the reaction of Boc-Val-OH and gemcitabine been completed. The reaction mixture was filtered, the filtrate was evaporated in vacuum and the residue was dissolved with 150 mL of ethyl acetate. The solution was successively washed with aqueous $NaHCO_3$ (5%, 100 mL ×3), aqueous $KHSO_4$ (5%, 100 mL ×3), aqueous NaCl (26%, 100 mL ×3), aqueous $NaHCO_3$ (5%, 100 mL ×3) and aqueous NaCl (26%, 100 mL ×3). The solution was dried with anhydrous Na_2SO_4 for 12 hrs, filtered, the filtrate was concentrated in vacuum and the residue was purified with silica gel column (CH_2Cl_2/CH_3OH, 35/1) to provide 3.15 g (68%) of the title compound as colorless powders. ESI-MS (m/z): 463 $[M + H]^{+;}$ ^{1}H NMR and ^{13}C NMR are shown in the Supporting Information.

4-Val-amino-1-[3,3-difluoro-4-hydroxy-5-(hydroxylmethyl)oxolan-2-yl]-pyrimidin-2-one (2)

At 0°C into a solution of 3.15 g (6.8 mmol) of 4-Boc-Val-amino-1-[3,3-difluoro-4-hydroxy-5-(hydroxylmethyl)oxolan-2-yl]pyrimidin-2-one (**1**) in 10 mL of anhydrous ethyl acetate, a solution of hydrogen chloride in anhydrous ethyl acetate (30 mL, 4M) was added, stirred at room temperature for 4 hrs and TLC (CH_2Cl_2/CH_3OH, 10/1) indicated the complete disappearance of **1**. The reaction mixture was repeatedly evaporated in vacuum to thoroughly remove the remaining hydrogen chloride, and finally the residue was titrated with anhydrous ether to provide 2.27 g (92%) of the title compound as colorless powders. ESI-MS (m/z): 363 $[M + H]^{+;}$ ^{1}H NMR and ^{13}C NMR are shown in the Supporting Information.

4-[Boc-Arg-Gly-Asp(OtBu)-val-amino]-1-[3,3-difluoro-4-hydroxy-5-(hydroxylme-thyl)oxolan-2-yl]pyrimidin-2-one (3)

At 0°C into a solution of 502 mg (1 mmol) of Boc-Arg-Gly-Asp(OtBu)-OH in 30 mL of anhydrous DMF, 135 mg (1 mmol) of HOBt and 247 mg (1.2 mmol) of DCC were added, stirred for 30 mins and then 434 mg (1.2 mmol) of 4-Val-amino-1-[3,3-difluoro-4-hydroxy-5-(hydroxyl-methyl)oxolan-2-yl]pyrimidin-2-one (**2**) was added. At 0°C, this reaction mixture was adjusted to pH 9 with NMM, stirred at room temperature for 10 hrs and TLC (CH_2Cl_2/CH_3OH, 10/1) indicated the reaction of Boc-Arg-Gly-Asp(OtBu)-OH and **2** been completed. The reaction mixture was filtered, the filtrate was evaporated in vacuum and the residue was extracted with 150 mL of butyl alcohol. The solution was successively washed with aqueous $NaHCO_3$ (5%, 100 mL ×3), aqueous $KHSO_4$ (5%, 100 mL ×3), aqueous NaCl (26%, 100 mL ×3), aqueous $NaHCO_3$ (5%, 100 mL ×3) and aqueous NaCl (26%, 100 mL ×3). The solution was dried with anhydrous Na_2SO_4 for 12 hrs, filtered, the filtrate was evaporated in vacuum and the residue was purified with C18 column (CH_3OH/H_2O, 4/6) to provide 270 mg (32%) of the title compound as colorless powders. ESI-MS (m/z): 847 $[M + H]^{+;}$ ^{1}H NMR and ^{13}C NMR are shown in the Supporting Information.

4-(Arg-Gly-Asp-Val-amino)-1-[3,3-difluoro-4-hydroxy-5-(hydroxylmethyl)oxo-lan-2-yl]pyrimidin-2-one (4)

At 0°C, 100 mg (0.118 mmol) of 4-[Boc-Arg-Gly-Asp-(OtBu)-Val-amino-1-[3,3-difluoro-4-hydroxy-5-(hydroxyl-methyl)oxolan-2-yl]pyrimidin-2-one (**3**) was treated with a solution of hydrogen chloride in anhydrous ethyl acetate (20 mL, 4M), and then at room temperature was stirred for 4 hrs and TLC (Cl_2CH_2/CH_3OH, 5/1) indicated the complete disappearance of **4**. The reaction mixture was repeatedly evaporated in vacuum to thoroughly remove the remaining hydrogen chloride, and finally the residue was titrated with anhydrous ether to provide 62.0 mg (76%) of the title compound as colorless powders. FT-MS (m/z) for $C_{26}H_{40}F_2N_{10}O_{10}$: calculated $[M + H]^+$, 691.29697; found $[M + H]^+$, 691.29587. HPLC purity: 99.5%. ^1H NMR and ^{13}C NMR are shown in the Supporting Information.

Characterization

FT-ICR-MS and qCID spectra

To reveal the molecular assembly of RGDV-gemcitabine, the FT-ICR-MS and qCID spectra were measured on Bruker 9.4 T solariX FT-ICR mass spectrometer equipped with an ESI/MALDI dual ion source. The measurement was performed by following the procedure of the equipment.

NOESY 2D NMR spectrum

To reveal the manner of the molecular assembly of RGDV-gemcitabine, the NOESY 2D NMR spectrum was measured on Bruker 800 MHz spectrometer. The measurement was performed by following the procedure of the equipment.

SEM, TEM and AFM feature

To image the nano-feature of RGDV-gemcitabine in the solid state, in water and in mouse plasma, the scanning electron microscopy (SEM), transmission electron microscopy (TEM) and atomic force microscopy (AFM) measurements were performed by following the procedure of the equipment.

Faraday-Tyndall effect, particle size and zeta potential tests

The nano-property of RGDV-gemcitabine in water was identified by Faraday-Tyndall effect, while the particle size and zeta potential were tested by following the procedure of particle size analyzer (Nano-ZS90; Malvern Instruments Ltd, Malvern, UK) and Zeta Potential Plus Analyzer (Brookhaven Instruments Corp, Holtsville, NY, USA). Aimed at this, the solution (0.1 μM) of RGDV-gemcitabine in the ultrapure water of pH 6.7 was prepared. The laser of 650 nm was for inducing Faraday-Tyndall effect.

Mesoscale simulation of nano-particle

With ChemDraw Ultra 10.0 (Cambridge Soft) and Materials Studio 3.2 (Accelrys, Inc. USA), the structure and conformation of RGDV-gemcitabine were generated, and then the conformation was entirely optimized with MS force module. To optimize the geometry, the maximum energy convergence and the maximum force were 2×10^{-5} kcal/mol and 0.001kcal/mol/Å, respectively. At 500 K with NVT ensemble, the molecular dynamic simulation was performed till reaching the equilibration. After equilibration, the structure was further optimized with MS Dmol^3 module to build a rigid coarse grain model of 3 connected spherical beads. This 3-spherical-bead model was randomly distributed (density: 0.15 g/cm^3) in a cubic box of 200×200×200 Å^3. At 298 K with NVT ensemble, a simulation of 15,000 ps was performed.

Bioassays

In vitro anti-proliferation assay

In T-25 flasks, all the stock cultures were grown. The suspensions of the freshly trypsinized HepG2, HCT-8, A549, MCF-7 and 95D cells were seeded in 96-well microtiter plates and the density was 5000 cells per well. The cells were in the high glucose-DMEM or the RPMI-1640 medium at 37ºC cultured for 4 hrs. The medium contained 10% (v/v) fetal calf serum, 60 μg/mL of penicillin and 100 μg/mL of streptomycin. After the addition of 25 μL of the solution (final concentration: 10 μM, 5 μM, 2.5 μM, 1 μM, 0.5 μM and 0.25 μM) of gemcitabine or RGDV-gemcitabine, the cells were cultured for 48 hrs, then 25 μL of MTT solution (5 μg/mL) was added and the cells were incubated for another 4 hrs. The medium was removed and MTT-formazan was dissolved in 100 μL of DMSO. On a microplate reader, the optical density (O.D.) was measured at 570 nm. The IC_{50} was calculated based on the survival curve and linear regression analysis. Each test was repeated in quadruplicate, and the results were expressed as mean ± SD μM.

In vivo anti-tumor assay

In this assay, ICR mice (male, 22±2 g) were used. For initiation, subcutaneous tumors S180 ascites tumor cells were obtained from the tumor-bearing mice that were serially transplanted once per week. By injecting 0.2 mL

saline containing 1×10^7 viable tumor cells under the skin on the right armpit, subcutaneous tumors were implanted, 5 days later the implanted mice were randomly divided into 5 groups (12 per group). To clarify the efficacy of RGDV-gemcitabine (0.084 μmol/kg/day, 0.84 μmol/kg/day and 8.4 μmol/kg/day), gemcitabine (84 μmol/kg/day) was used as positive control, while NS (10 mL/kg/day) was used as negative control. The mice in the groups were orally given NS or gemcitabine or RGDV-gemcitabine every 3 days for 12 days. During the 12 days, the body-weight of all mice was recorded every day, and 3 hrs after the last administration all mice were weighed, sacrificed by diethyl ether anesthesia and 1 mL of fresh blood was collected. Then the tumors and organs were dissected and weighed immediately.

In vivo serum ALT/GPT assay

Serum alanine aminotransferase (ALT/GPT) was measured by using the procedure of ALT/GPT kit (Nanjing Jiancheng Bioengineering Institute, PR China). To get serum, 0.5 mL blood was collected from S180 mice receiving in vivo anti-tumor assay, which were treated with NS (10 mL/kg/day) or gemcitabine (84 μmol/kg/day) or RGDV-gemcitabine (8.4 μmol/kg/day). At 4°C, the blood was centrifuged (1000 rpm) for 10 mins to prepare serum. To all wells, 20 μL matrix solution was added. To each standard well, 5 μL standard solution was added. To each testing well, 5 μL serum of S180 mice treated with NS or gemcitabine or RGDV-gemcitabine was added. The well was at 37°C incubated for 30 mins. To all wells, 20 μL of dinitrophenylhydrazine was added and the well was incubated at 37°C for 20 mins. To each well, 200 μL of sodium hydroxide solution (0.4 M) was added, and the plate was gently tapped for 15 mins to ensure thorough mixing. The plate was read at 510 nm with microtiter plate reader to record O.D. value. Based on the standard curve, serum ALT/GPT was calculated.

In vivo serum AST/GOT assay

With a similar procedure to ALT/GPT assay and using aspartic aminotransferase (AST/GOT) kit (Nanjing Jiancheng Bioengineering Institute, PR China), serum AST/GOT of S180 mice treated with NS (10 mL/kg/day) or gemcitabine (84 μmol/kg/day) or RGDV-gemcitabine (8.4 μmol/kg/day) were measured and calculated.

In vivo serum Cr assay

Serum creatinine (Cr) was measured by following the procedure of the kit (Nanjing Jiancheng Bioengineering Institute, PR China). To get serum, 0.5 mL blood was collected from S180 mice receiving in vivo anti-tumor assay, which were treated with NS (10 mL/kg/day) or gemcitabine (84 μmol/kg/day) or RGDV-gemcitabine (8.4 μmol/kg/day). At 4°C, the blood was centrifuged (1000 rpm) for 10 mins. To each standard well, 6 μL of the standard solution was added. To each testing well, 6 μL of serum from S180 mice treated with NS or gemcitabine or RGDV-gemcitabine was added. To the well, 60 μL enzyme solution A was added. The well was incubated at 37°C for 5 mins and was read at 546 nm by using a microtiter plate reader to record O.D. value (A_1). The well was at 37°C incubated for 30 mins. To the well, 60 μL enzyme solution B were added. The well was incubated at 37°C for 5 mins and read at 546 nm by using a microtiter plate reader to record O.D. value (A_2). The contents of Cr in samples were calculated by using the common equation.

In vivo serum BUN assay

The measurement of blood urea nitrogen (BUN) was performed by following the procedure of the kit (Shanghai Lianshuo Biological Technology Co., Ltd, PR China). To get serum, 0.5 mL blood was collected from S180 mice receiving in vivo anti-tumor assay, which were treated with NS (10 mL/kg/day) or gemcitabine (84 μmol/kg/day) or RGDV-gemcitabine (8.4 μmol/kg/day). At 4°C, the blood was centrifuged (3000 rpm) for 10 mins. To each standard well, 50 μL standard solution and 50 μL streptavidin-horseradish peroxidase (streptavidin-HRP) were added. To each testing well, 40 μL serum from S180 mice treated with NS or gemcitabine or RGDV-gemcitabine, 10 μL anti-BUN-antibody and 50 μL streptavidin-HRP were successively added. At 37ºC, the well was incubated for 60 mins, and then washed 5 times. For coloration to the well 50 μL, chromogen solution A and 50 μL chromogen solution B of the kit were added, and the well was at 37ºC incubated in dark for 15 mins. To stop the reaction, the well received 50 μL stop solution of the kit. The O.D. value was measured at 450 nm within 15 mins of the addition of the stop solution. By using standard curve, serum BUN was calculated.

ESI(+)-FT-MS analysis of homogenate extracts

To examine tumor-targeting effect

To examine the targeting action the tumor tissue, blood, brain, heart, kidney, liver and spleen of S180 mice treated

with NS (10 mL/kg/day) or RGDV-gemcitabine (8.4 μmol/kg/day) were homogenized, the homogenates were extracted with methanol and the extracts received ESI (+)-FT-MS analysis.

In the preparation of blood extract, the blood of NS or RGDV-gemcitabine-treated mice received ultrasonication (30 mins) and centrifugation (4000 rpm/min, 15 mins) to collect the supernatant. The supernatant was blown with nitrogen to dry, and the residue was dissolved in chromatographic pure methanol (200 μL methanol per g of blood) for FT-ICR-MS analysis.

To prepare the extracts of the tumor tissue or the brain or the heart or the kidney or the liver or the spleen of NS or RGDV-gemcitabine-treated S180 mice, the tumor was in 1 mL of ultrapure water to homogenize, then received ultrasonication (30 mins) and centrifugation (4000 rpm/min, 15 mins). The supernatant was blown with nitrogen to dry, and the residue was dissolved in chromatographic pure methanol (200 μL methanol per g of tumor tissue or organ) for FT-ICR-MS analysis.

To examine tumor-targeting release

To prepare the extract of the tumor tissue of RGDV-gemcitabine-treated S180 mice, the tumor tissue was in 1 mL of ultrapure water to homogenize, then received ultrasonication (30 mins) and centrifugation (4000 rpm/min, 15 mins). The supernatant was blown with nitrogen to dry, and the residue was dissolved in chromatographic pure methanol (200 μL methanol per g of tumor tissue) for FT-ICR-MS analysis.

Results

RGDV-gemcitabine could be optionally prepared

The synthesis consisted of 9-step reactions (Figure 2); the yields of 9-step reactions ranged from 32% to 92% and the HPLC purity of RGDV-gemcitabine was 99.5%. Synthetic data demonstrate that RGDV-gemcitabine could be optionally provided by using this route for supporting the afterward investigations.

RGDV-gemcitabine overcomes drug resistance of gemcitabine

Dipyridamole greatly decreasing the anti-proliferative efficacy of gemcitabine against human cancer lines was well documented and commonly used to evaluate drug resistance.[40–42] In this regard, the IC_{50} of gemcitabine alone, gemcitabine plus dipyridamole, RGDV-gemcitabine alone and RGDV-gemcitabine plus dipyridamole against the proliferation of A549 cells were determined by MTT assay. Figure 3 shows that dipyridamole induces the IC_{50} of gemcitabine from 2.5 μM increased to 48.0 μM (19.2-fold increase), but has little influence on the IC_{50} of RGDV-gemcitabine (from 2.5 μM increased to 4.7 μM, only 1.9-fold increase). This means that the modification of Arg-Gly-Asp-Val successively reverses dipyridamole-induced drug resistance. Therefore, RGDV-gemcitabine has no resistance and is suitable for further investigations.

Self-assembly of RGDV-gemcitabine

FT(+)-MS and qCID spectra defined trimer

The self-assembly of small molecule has been well documented.[43–45] Here, the self-assembly of RGDV-gemcitabine in ultrapure water (1 nM) was explored with its FT(+)-MS spectrum. Figure 4A shows an ion peak at 691.2956, the mass of a monomer plus H, and an ion peak at 1036.4449, the mass of the bivalent positive ion of a trimer plus H. To clarify the relationship between the trimer and the monomer, a qCID spectrum of the trimer was recorded. Figure 4B indicates that in FT-MS condition the trimer can be split to an ion at 691.2908, the mass of a monomer plus H, and an ion at 1381.5719, the mass of a dimer plus H. This means that in water the trimer is the smallest species of RGDV-gemcitabine.

NOESY 2D ^{1}HNMR spectrum defined trimerization manner

To know how RGDV-gemcitabine forms a trimer, its NOESY 2D ^{1}HNMR spectrum was recorded. Figure 4C shows two interesting cross-peaks. The cross-peaks are marked with red circles. According to the knowledge of NOESY, cross-peak 1 is from the interaction of the H of the CO_2H of Asp residue of the first molecule and the H of CH_2CH of the sugar ring of the second molecule, cross-peak 2 is from the interaction of the H of the NH_2 of guanidine of Arg residue of the third molecule and the H of CH_2CH of the sugar ring of the first molecule. This means that the distance between these H is less than 4Å.

NOESY 2D ^{1}HNMR spectrum defined a W-like conformation for trimer

Based on this, the monomer of RGDV-gemcitabine was first energy minimized, and then the assembly of three energy-minimized monomers was manually accessed to form a trimer. This operation leads the trimer to have a W-like conformation (Figure 4D). With this conformation,

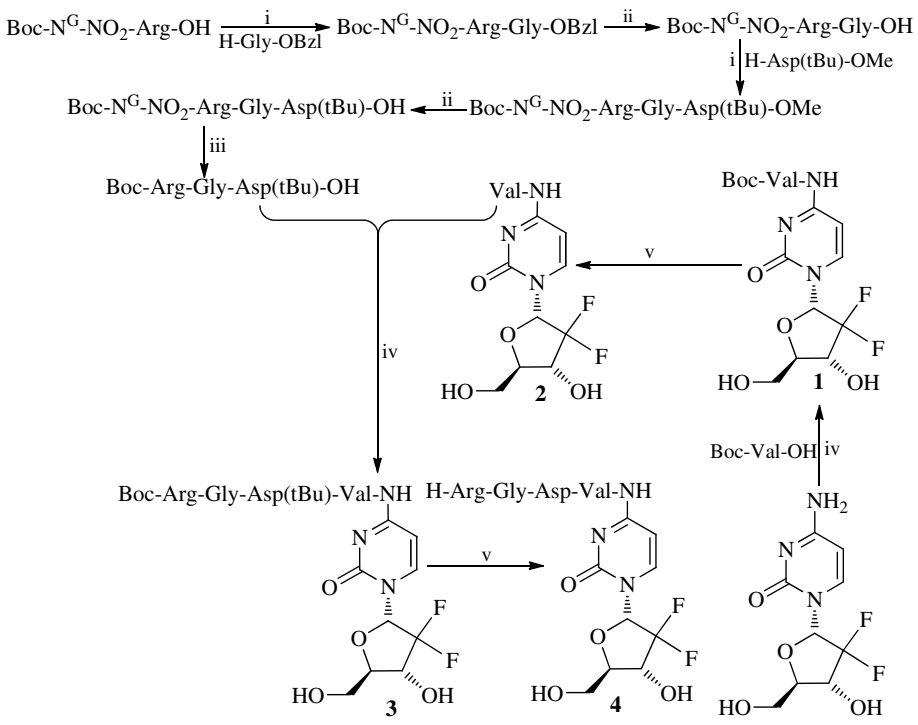

Figure 2 Synthetic route of RGDV-gemcitabine (**4**)[a].
Notes: [a]Reagents: i) DCC, HOBt, NMM and THF; ii) CH_3OH and aqueous NaOH (4 M); iii) CH_3OH and Pd/C; iv) DCC, HOBt and DMF; v) Hydrochloride in ethyl acetate (4 M).
Abbreviations: DCC, dicyclohexylcarbodiimide; HOBt, N-hydroxybenzotriazole; NMM, N-methylmorpholine; THF, tetrahydrofuran; DMF, N,N-dimethylformamide; RGDV-gemcitabine, 4-(Arg-Gly-Asp-Val-amino)-1-[3,3-difluoro-4-hydroxy-5-(hydroxylmethyl)oxo-lan-2-yl]pyrimidin-2-one.

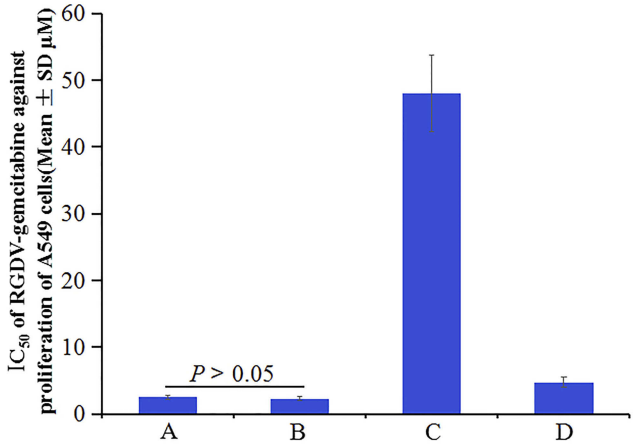

Figure 3 IC_{50} of gemcitabine and RGDV-gemcitabine against the proliferation of A549 cells. (**A**) IC_{50} of gemcitabine alone against the proliferation of A549 cells; (**B**) IC_{50} of RGDV-gemcitabine alone against the proliferation of A549 cells; (**C**) IC_{50} of gemcitabine plus dipyridamole against the proliferation of A549 cells; (**D**) IC_{50} of RGDV-gemcitabine plus dipyridamole against the proliferation of A549 cells, n=3.
Abbreviations: RGDV-gemcitabine, 4-(Arg-Gly-Asp-Val-amino)-1-[3,3-difluoro-4-hydroxy-5-(hydroxylmethyl)oxo- lan-2-yl]pyrimidin-2-one.

the moiety of gemcitabine in RGDV-gemcitabine could be shielded to prevent deaminase (CDA) and deoxycytidilate deaminase (dCMP-DA) approaching, thereby avoiding the enzymes-induced inactivation.[3,46]

Nano-solution

Aqueous RGDV-gemcitabine showing faraday-Tyndall effect

The nano-property of aqueous RGDV-gemcitabine was explained by Faraday-Tyndall effect, particle size and zeta potential. Aimed at this, a solution (0.1 μM) of RGDV-gemcitabine in the ultrapure water of pH 6.7 was prepared. The laser of 650 nm was used to induce Faraday-Tyndall effect. Figure 5A–D shows that with laser radiation only the solution of RGDV-gemcitabine in ultrapure water of pH 6.7 shows Faraday-Tyndall effect. This means that aqueous RGDV-gemcitabine is nano-solution.

Particle size and zeta potential stabilize the nano-solution

Particle size and zeta potential were tested for supporting the stability of the nano-solution of RGDV-gemcitabine in ultrapure water of pH 6.7. Figure 5E shows that during 7 days the size of nano-particles falls within a range of ~90–100 nm. Thus the size of the nano-particles formed by RGDV-gemcitabine in water is held in a limited range, and this could stabilize the nano-solution. Figure 5F shows that on 7th day the apparent zeta potential is −52.3 mv. This means that the surface of the nano-particles is surrounded by dense negative

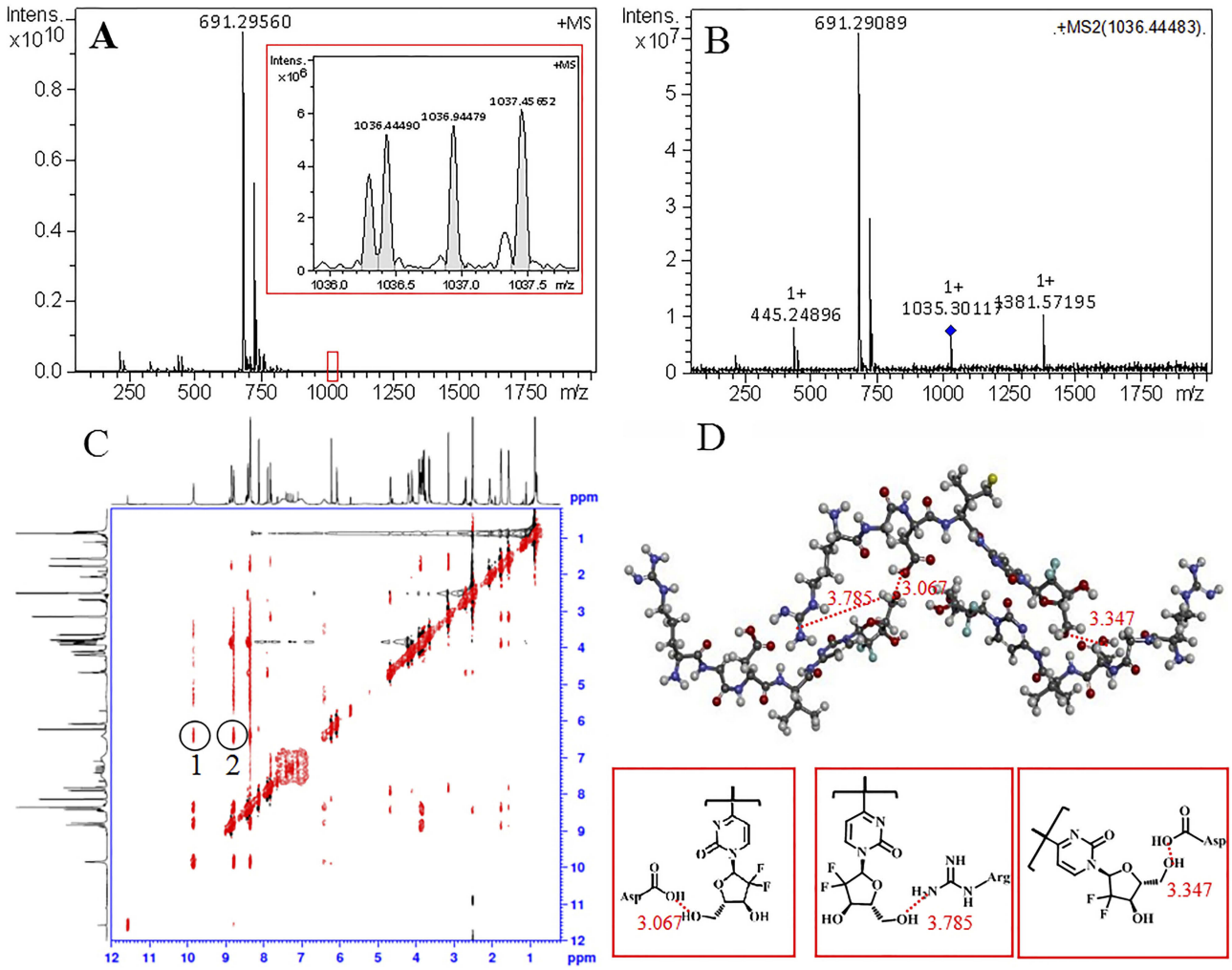

Figure 4 (**A**) FT-MS spectrum gives RGDV-gemcitabine an ion peak of monomer and an ion peak of trimer; (**B**) qCID spectrum of the trimer gives an ion peak of monomer and an ion peak of dimer; (**C**) NOESY 2D ^{1}H NMR spectrum gives two cross-peaks that defines the approach manner of RGDV-gemcitabine forming trimer; (**D**) to fit the NOESY 2D ^{1}H NMR spectrum, the trimer of RGDV-gemcitabine should possess butterfly-like conformation.
Abbreviations: RGDV-gemcitabine, 4-(Arg-Gly-Asp-Val-amino)-1-[3,3-difluoro-4-hydroxy-5-(hydroxylmethyl)oxo-lan-2-yl]pyrimidin-2-one.

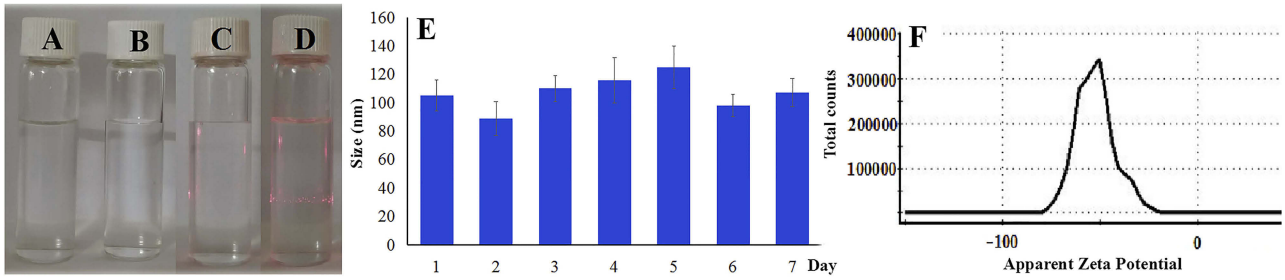

Figure 5 Faraday-Tyndall effect, particle size and zeta potential of aqueous RGDV-gemcitabine. (**A**) Without radiation of 650 nm laser, the ultrapure water of pH 6.7 shows no Faraday-Tyndall effect; (**B**) Without radiation of 650 nm laser, the solution of RGDV-gemcitabine in the ultrapure water of pH 6.7 (0.1 μM) shows no Faraday-Tyndall effect; (**C**) With radiation of 650 nm laser, the ultrapure water of pH 6.7 shows no Faraday-Tyndall effect; (**D**) With radiation of 650 nm laser, the solution of RGDV-gemcitabine in the ultrapure water of pH 6.7 (0.1 μM) shows Faraday-Tyndall effect; (**E**) 7 days' size of the nano-particles of RGDV-gemcitabine in ultrapure water of pH 6.7 (0.1 μM); (**F**) On 7th day, the zeta potential of the nano-particles of RGDV-gemcitabine in ultrapure water of pH 6.7 (0. μM).
Abbreviations: RGDV-gemcitabine, 4-(Arg-Gly-Asp-Val-amino)-1-[3,3-difluoro-4-hydroxy-5-(hydroxylmethyl)oxo-lan-2-yl]pyrimidin-2-one.

charge, and the negative charge could strongly repel each other to prevent the particles from aggregation, thereby to stabilize the nano-solution.

Nano-species

SEM imaged nano-blocks of RGDV-gemcitabine

The nano-species of the lyophilized powders from a solution of RGDV-gemcitabine in ultrapure water (pH 6.7, 0.01 μM) was visualized by SEM. Figure 6A shows that the lyophilized powders from the solution of RGDV-gemcitabine in ultrapure water are well-dispersed nano-blocks, and the size of more than 90% blocks is less than 105 nm^3.

TEM imaged nano-particles of RGDV-gemcitabine

The nano-species of RGDV-gemcitabine in ultrapure water (pH 6.7, 0.01 μM) was visualized by TEM. Figure 6B shows that in ultrapure water RGDV-gemcitabine forms nano-particles, and the diameter of more than 85% particles is less than 100 nm. Of them, approximately 60% particles have the diameter less than 60 nm.

AFM imaged nano-particles of RGDV-gemcitabine

The nano-species of RGDV-gemcitabine in ultrapure water (pH 6.7, 0.01 μM) and mouse serum (0.01 μM) was visualized by AFM. Figure 6C shows that in ultrapure water RGDV-gemcitabine forms nano-particle, and the height of the nano-particles is less than 18 nm. Figure 6E shows that in mouse serum, RGDV-gemcitabine forms nano-particle, and the height of the nano-particle is less than 8 nm, even though the mouse serum gives no comparable nano-particle (Figure 6D).

Mesoscale simulation predicted composition of nano-particle

To predict the composition of the nanoparticle of RGDV-gemcitabine, a simulation was performed by using the mesoscale simulation software. Figure 7 shows the course of mesoscale simulation. First, the optimized structure of RGDV-gemcitabine is converted to a coarse grain model of 3 connected spherical beads. Second, in a cubic box of 200×200×200 $Å^3$, this coarse grain model is randomly distributed with a density of 0.15 g/cm^3. Finally, a 15,000 ps simulation is performed on this system at 298 K using NVT ensemble, and 87 trimers could construct a nano-particle of 35 nm in diameter. This means that mesoscale simulation could be generally used to estimate the molecular number of an optional nano-particle of RGDV-gemcitabine.

Activities

RGDV-gemcitabine inhibits the proliferation of cancer cells

The in vitro anti-tumor activity was reflected with IC_{50} of RGDV-gemcitabine inhibiting the proliferation of cancer cells. Figure 8A shows that the IC_{50} values of gemcitabine

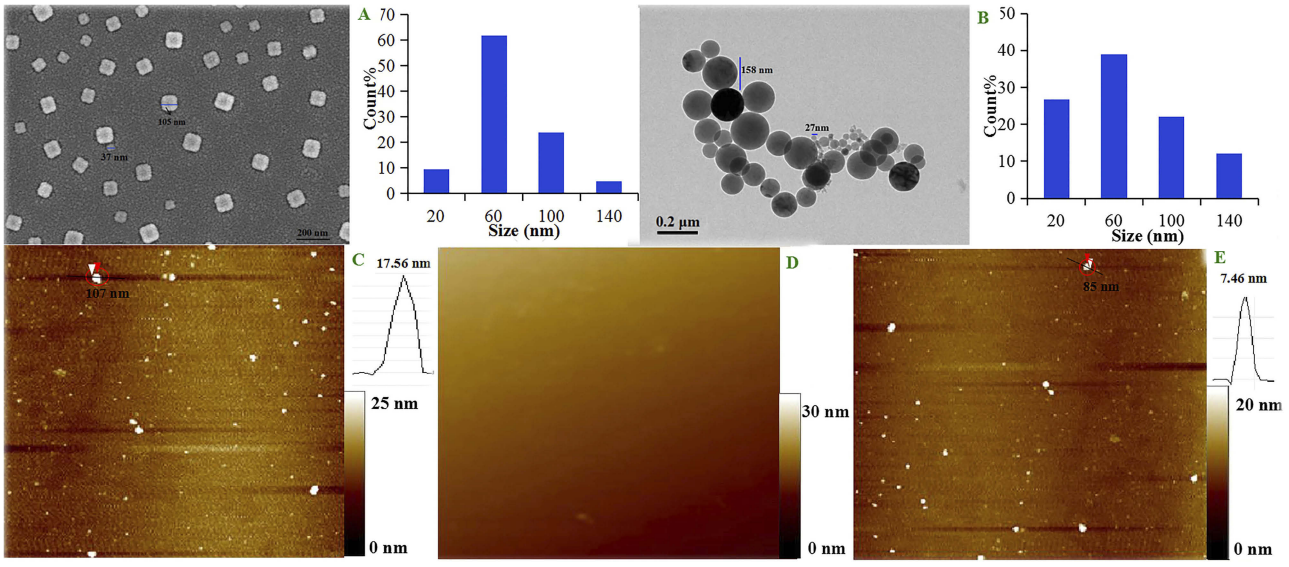

Figure 6 Nano-feature of RGDV-gemcitabine. (**A**) Nano-feature of the powders lyophilized from a solution of RGDV-gemcitabine in ultrapure water (pH 6.7, 0.01 μM) imaged with SEM; (**B**) nano-feature of RGDV-gemcitabine in ultrapure water (pH 6.7, 0.01 μM) imaged with TEM; (**C**) nano-feature of RGDV-gemcitabine in ultrapure water (pH 6.7, 0.01 μM) imaged with AFM (**C**); (**D**) nano-feature of mouse serum imaged with AFM; (E) nano-feature of RGDV-gemcitabine in mouse serum (0.01 μM) imaged with AFM.

Abbreviations: SEM, scanning electron microscopy; TEM, transmission electron microscopy; AFM, atomic force microscopy; RGDV-gemcitabine, 4-(Arg-Gly-Asp-Val-amino)-1-[3,3-difluoro-4-hydroxy-5-(hydroxylmethyl)oxo- lan-2-yl]pyrimidin-2-one.

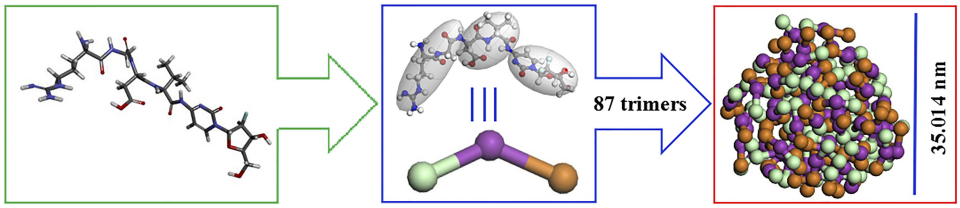

Figure 7 Mesoscale simulation course of RGDV-gemcitabine forming a sized particle.
Abbreviations: RGDV-gemcitabine, 4-(Arg-Gly-Asp-Val-amino)-1-[3,3-difluoro-4-hydroxy-5-(hydroxylmethyl)oxo-lan-2-yl]pyrimidin-2-one.

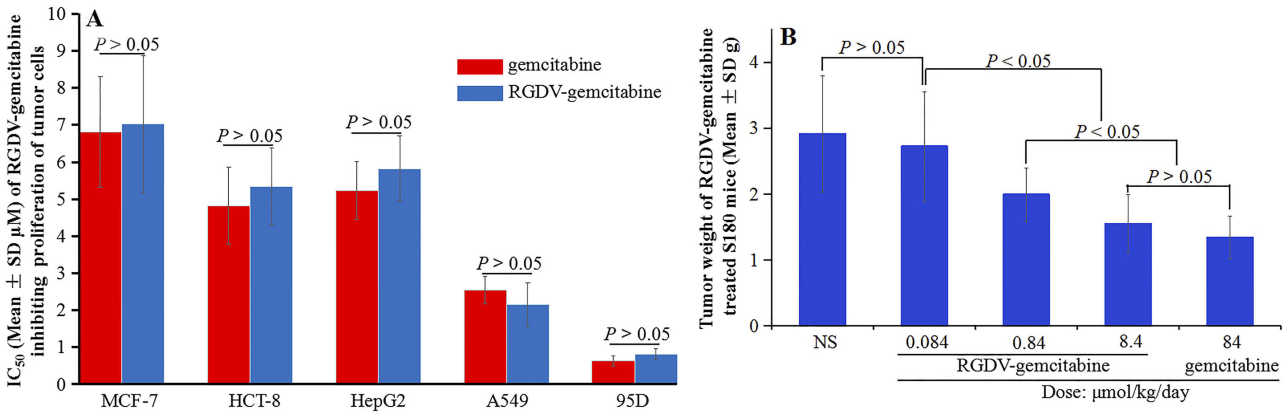

Figure 8 Anti-tumor activities of RGDV-gemcitabine. (**A**) IC_{50} of gemcitabine and RGDV-gemcitabine inhibiting the proliferation of MCF-7, HCT-8, A549, 95D and HepG2 cells, n=9; (**B**) tumor weight of gemcitabine and RGDV-gemcitabine treated S180 mice, n=12.
Abbreviations: RGDV-gemcitabine, 4-(Arg-Gly-Asp-Val-amino)-1-[3,3-difluoro-4-hydroxy-5-(hydroxylmethyl)oxo-lan-2-yl]pyrimidin-2-one.

and RGDV-gemcitabine inhibiting the proliferation of MCF-7, HCT-8, A549, 95D and HepG2 cells have no significant difference. This means that Arg-Gly-Asp-Val modification does not change the in vitro anti-tumor activity of gemcitabine.

RGDV-gemcitabine dose-dependently inhibits tumor growth

The in vivo anti-tumor assay was performed on S180 tumor-bearing mouse model. During the 12 days, the mice were orally given gemcitabine (84 μmol/kg/day) or RGDV-gemcitabine (0.084 μmol/kg/day, 0.84 μmol/kg/day and 8.4 μmol/kg/day) every 3 days. Figure 8B shows that RGDV-gemcitabine dose-dependently inhibits the tumor growth, the minimal effective dose is 0.84 μmol/kg/day and the tumor weight of S180 mice treated with 8.4 μmol/kg/day of RGDV-gemcitabine is equal to that of the mice treated with 84 μmol/kg/day of gemcitabine. This means that Arg-Gly-Asp-Val modification results in the in vivo activity of gemcitabine having 10-fold increase.

Toxicity

RGDV-gemcitabine does not injure the liver

To estimate the toxicity of gemcitabine and RGDV-gemcitabine to liver, the serum ALT/GPT and AST/GOT of S180 tumor-bearing mice treated by NS or 8.4 μmol/kg/day of RGDV-gemcitabine or 84 μmol/kg/day of gemcitabine were measured by using the corresponding kits. Figure 9A and B shows that the serum ALT/GPT and AST/GOT of RGDV-gemcitabine-treated S180 mice are equal to those of NS-treated mice, while the serum ALT/GPT and AST/GOT of gemcitabine-treated S180 mice are significantly higher than those of NS-treated mice. Therefore, gemcitabine, but not RGDV-gemcitabine, injures the liver of tumor-bearing mice.

RGDV-gemcitabine does not injure the kidney

To estimate the toxicity of gemcitabine and RGDV-gemcitabine to kidney, the serum Cr and BUN of S180 tumor-bearing mice treated by NS or 8.4 μmol/kg/day of RGDV-gemcitabine or 84 μmol/kg/day of gemcitabine were measured by using the corresponding kits. Figure 9C and D shows that the serum Cr and BUN of S180 mice treated by RGDV-gemcitabine are equal to those of NS-treated mice, while the serum Cr and BUN of S180 mice treated by gemcitabine are significantly higher than those of NS-treated mice. Therefore, gemcitabine, but not RGDV-gemcitabine, injures the kidney of tumor-bearing mice.

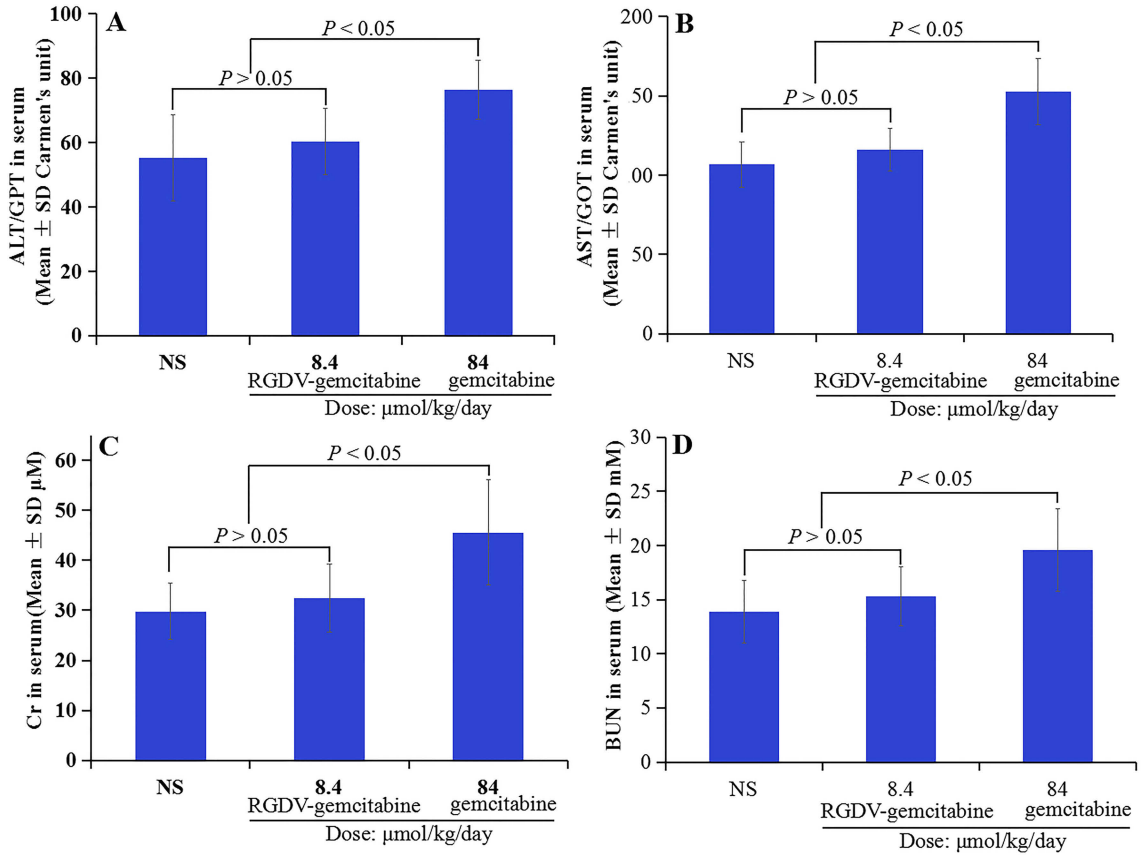

Figure 9 Serum ALT/GPT (**A**), AST/GOT (**B**), Cr (**C**) and BUN (**D**) of S180 mice treated by 8.4 μmol/kg/day of RGDV-gemcitabine and 84 μmol/kg/day of gemcitabine, n=12.

Abbreviations: ALT/GPT, alanine aminotransferase; AST/GOT, aspartic aminotransferase; Cr, creatinine; BUN, blood urea nitrogen; RGDV-gemcitabine, 4-(Arg-Gly-Asp-Val-amino)-1-[3,3-difluoro-4-hydroxy-5-(hydroxylmethyl)oxo-lan-2-yl]pyrimidin-2-one.

RGDV-gemcitabine does not injure the marrow

To estimate the toxicity of gemcitabine and RGDV-gemcitabine to marrow, the red blood cells, white blood cells, platelets and neutrophil of S180 mice treated by 8.4 μmol/kg/day of RGDV-gemcitabine and 84 μmol/kg/day of gemcitabine were counted. Figure 10A–D shows that the count of the red blood cells, white blood cells, platelets and neutrophil of S180 mice treated by RGDV-gemcitabine are equal to those of NS-treated mice, while the count of the red blood cells, white blood cells, platelets and neutrophil of S180 mice treated by gemcitabine are significantly lower than those of NS-treated mice. Therefore, gemcitabine, but not RGDV-gemcitabine, injures the marrow of S180 tumor-bearing mice.

Tumor target and release

RGDV-gemcitabine targets tumor tissue

It has been demonstrated that RGD-peptide-containing molecules could form nanoparticles having targeting action;[43–45] therefore, we hypothesized that by forming nano-particles, RGDV-gemcitabine could target the tumor tissue of the treated S180 tumor-bearing mice. In this regard, the extracts of the homogenates of the tumor tissue, the brain, the heart, the lung, the liver, the spleen, the kidney and the blood of S180 mice treated with NS and 8.4 μmol/kg/day of RGDV-gemcitabine received FT(+)-MS spectrum analysis. Figure 11A and C shows that the FT(+)-MS spectra of the extracts of the blood and tumor tissue, but not the other organs, of the mice treated by RGDV-gemcitabine, but not NS, give the ion peak at 691.3013 and 691.3002 (the mass of RGDV-gemcitabine plus H), respectively. These data not only suggest that in blood circulation RGDV-gemcitabine is delivered without degradation but also emphasize that RGDV-gemcitabine is capable of targeting tumor tissue.

RGDV-gemcitabine releases pharmacophores in tumor tissue

Figure 11 is the FT(+)-MS spectrum of the extract of tumor tissue of RGDV-gemcitabine-treated mice. In addition to the ion peak at 691.3002 (the mass of RGDV-gemcitabine plus

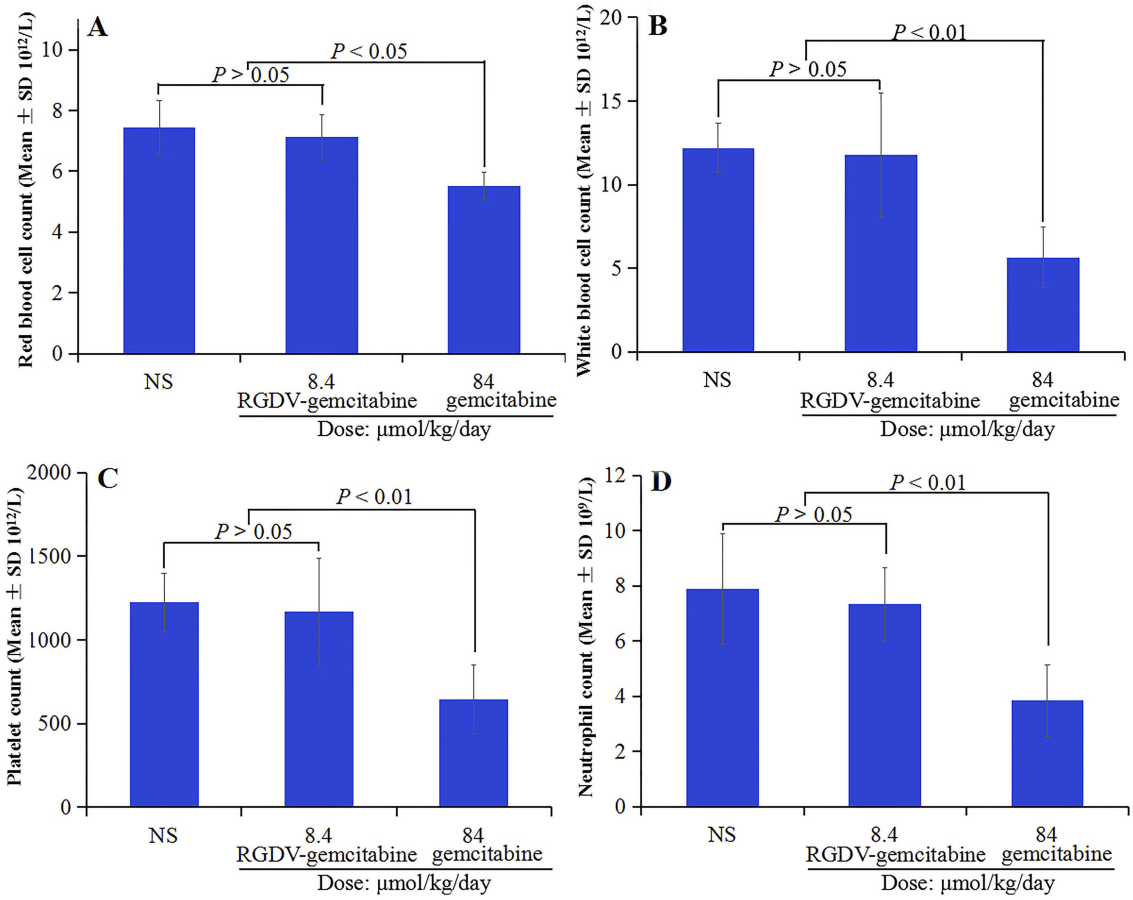

Figure 10 Count of red blood cells, white blood cells, platelets and neutrophil of the treated S180 mice. (**A**) Count of red blood cells; (**B**) count of white blood cells; (**C**) count of platelets; (**D**) count of neutrophil, n=12.

Abbreviations: RGDV-gemcitabine, 4-(Arg-Gly-Asp-Val-amino)-1-[3,3-difluoro-4-hydroxy-5-(hydroxylmethyl)oxo-lan-2-yl]pyrimidin-2-one.

H), the spectrum also gives the ion peaks at 468.2115 (the mass of Arg-Gly-Asp-Val plus H), at 557.1731 (the mass of GDV-gemcitabine plus Na), at 478.1694 (the mass of DV-gemcitabine plus H), at 363.2060 (the mass of V-gemcitabine plus H) and at 264.0771 (the mass of gemcitabine plus H). These data suggest that in tumor tissue, RGDV-gemcitabine is capable of releasing pharmacophores.

Discussion

The modification of gemcitabine with Arg-Gly-Asp-Val leads to a rational design and practicable synthesis of RGDV-gemcitabine. As a novel derivative of gemcitabine in mouse plasma, its half-life is 17-fold longer than that of gemcitabine. The prolonged half-life greatly benefits the biological behavior of RGDV-gemcitabine. Dipyridamole induces the IC_{50} of gemcitabine against the proliferation of A549 cells having 19.5-fold increase, but has little influence on the IC_{50} of RGDV-gemcitabine. The drug resistance of gemcitabine is overcome by RGDV-gemcitabine. The IC_{50} values of gemcitabine and RGDV-gemcitabine inhibiting the proliferation of MCF-7, HCT-8, A549, 95D and HepG2 cells have no significant difference. Arg-Gly-Asp-Val modification does not change the in vitro anti-tumor activity of gemcitabine. On S180 tumor-bearing mouse model, RGDV-gemcitabine dose-dependently inhibits tumor growth. The minimal effective dose and the activity of RGDV-gemcitabine are 100-fold lower and 10-fold higher than that of gemcitabine, respectively. RGDV-gemcitabine, but not gemcitabine, does not injure the liver, the kidney and the marrow of the treated tumor-bearing mice.

The biological advantages of RGDV-gemcitabine to gemcitabine are attributed to its nano-property. FT(+)-MS, qCID and NOESY 2D ^{1}H NMR spectra identify that the self-assembly of RGDV-gemcitabine leads to the formation of W-like trimer. The SEM and TEM consistently evidence that the nano-particles less than 100 nm in diameter are a characteristic form of RGDV-gemcitabine. It is well accepted that this kind of nano-particle is not only capable of escaping

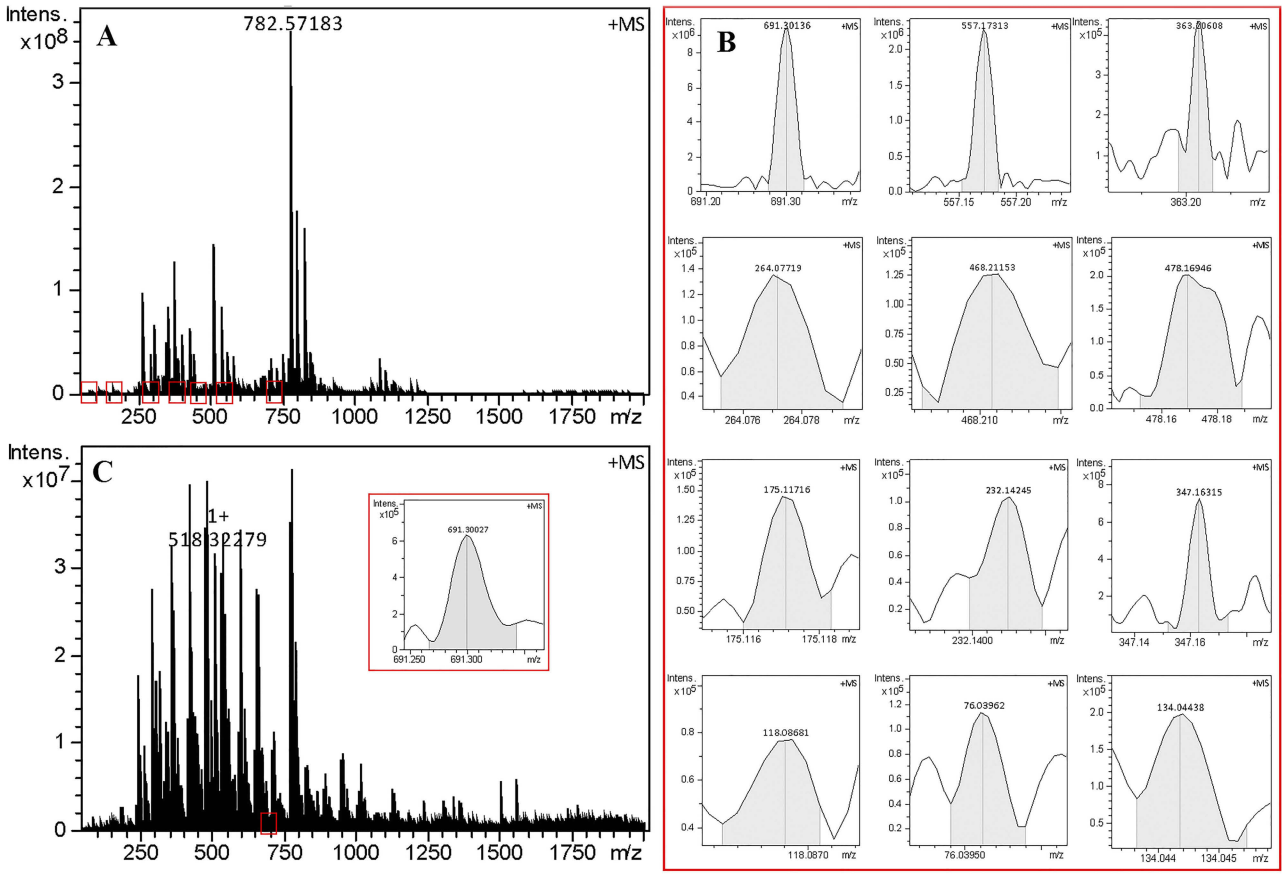

Figure 11 FT(+)-MS spectrum of the extract of the homogenate of tumor tissue and blood of S180 mice treated with 8.4 μmol/kg/day of RGDV-gemcitabine. (**A**) FT(+)-MS spectrum of the extract of the homogenate of the tumor tissue; (**B**) locally amplified spectra of Arg-Gly-Asp-Val plus H at 468.2117, Arg-Gly-Asp plus H at 347.1631, Arg-Gly plus H at 232.1424, Arg plus H at 175.1176, Gly plus H at 76.0396, Asp plus H at 134.0443, Val plus H at 118.0868, RGDV-gemcitabine plus H at 691.3013, GDV-gemcitabine plus Na at 557.1737, DV-gemcitabine plus H at 478.1694, V-gemcitabine plus H at 363.2060 and gemcitabine plus H at 264.0771; (**C**) FT(+)-MS spectrum of the extract of the homogenate of the blood and amplified spectrum of RGDV-gemcitabine plus H at 691.3002.

Abbreviations: RGDV-gemcitabine, 4-[Arg-Gly-Asp-Val-amino-1-[3,3-difluoro-4-hydroxy-5- (hydroxylme-thyl)oxolan-2-yl]pyrimidin-2-one; GDV-gemcitabine, 4-[Gly-Asp-Val-amino-1-[3,3-difluoro-4-hydroxy-5-(hydroxylme-thyl)oxolan-2-yl]pyrimidin-2-one; DV-gemcitabine, 4-[Arg-Gly-Asp-Val-amino-1-[3,3-difluoro-4- hydroxy-5-(hydroxylme-thyl)oxolan-2-yl]pyrimidin-2-one.

macrophage from swallowing but also can be delivered in blood circulation without metabolism. These are evidenced by FT(+)-MS spectrum analysis. The FT(+)-MS spectrum of blood extract of the mice treated with RGDV-gemcitabine undeniably and exclusively gives an ion peak at 691.3013 (the mass of RGDV-gemcitabine plus H).

The AFM evidences that in mouse serum the height of the nao-particle is 8 nm only. Such small nano-particle should specifically cross cancer cell membrane, selectively enters into tumor tissue and thereby shows tumor-targeting effect. These are evidenced by FT(+)-MS spectrum analysis. The FT(+)-MS spectrum of the extract of the tumor, but not the other organs, of the mice treated with RGDV-gemcitabine undeniably gives an ion peak at 691.3002 (the mass of RGDV-gemcitabine plus H), defines that RGDV-gemcitabine has tumor-targeting effect and emphasizes that RGDV-gemcitabine does not enter the liver, the kidney and the marrow of the treated tumor-bearing mice, therefore shows no toxicity to liver, kidney and marrow.

FT(+)-MS analysis of Figure 11B for tumor extract indicates that in addition to the ion peak at 691.3002, the spectrum also gives 11 ion peaks: Arg-Gly-Asp-Val plus H, Arg-Gly-Asp plus H, Arg-Gly plus H, Arg plus H, Gly plus H, Asp plus H, Val plus H, GDV-gemcitabine plus Na, DV-gemcitabine plus H, V-gemcitabine plus H and gemcitabine plus H. The ion peak of RGDV-gemcitabine plus H with these 11 ion peaks together explore a release course of RGDV-gemcitabine in tumor tissue. This course is graphically summarized in Figure 12.

Conclusion

In summary, the modification of gemcitabine with Arg-Gly-Asp-Val leads to the rational design and practicable

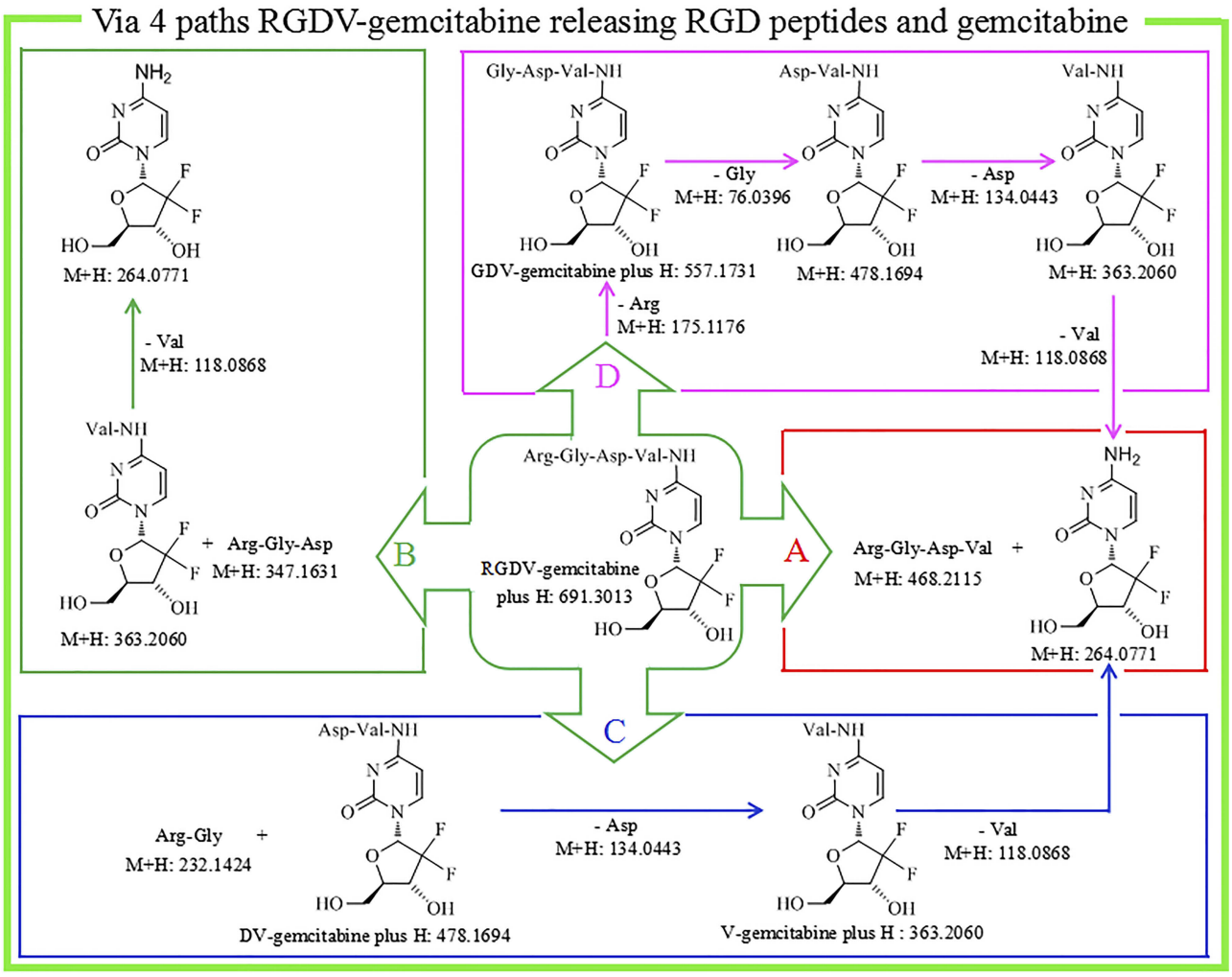

Figure 12 In the tumor tissue, RGDV-gemcitabine could release gemcitabine and Arg-Gly-Asp-Val via path A, B, C and D.
Abbreviations: RGDV-gemcitabine, 4-(Arg-Gly-Asp-Val-amino)-1-[3,3-difluoro-4-hydroxy-5- (hydroxylmethyl)oxolan-2-yl]pyri-midin-2-one; GDV-gemcitabine, 4-(Gly-Asp-Val-amino)-1-[3,3-difluoro-4-hydroxy-5-(hydroxylme-thyl)oxolan-2-yl]pyrimidin-2-one; DV-gemcitabine, 4-(Asp-Val-amino)-1-[3,3-difluoro-4-hydroxy-5-(hydroxylme-thyl) oxolan-2-yl]pyrimidin-2-one; V-gemcitabine, 4-(Val-amino)-1-[3,3-difluoro-4-hydroxy-5-(hydroxylme-thyl)oxolan-2-yl]pyrimi-din-2-one.

synthesis of RGDV-gemcitabine, a novel derivative of gemcitabine. By forming small and uniform nano-particle, RGDV-gemcitabine is capable of escaping macrophage from swallowing and delivery in blood circulation without metabolism, thereby to prolong the half-life and overcome drug resistance. Such nano-particle can specifically cross cancer cell membrane and selectively enter into tumor tissue, and thereby show tumor-targeting effect. The tumor-targeting action grants RGDV-gemcitabine high efficacy, low toxicity and specific manner of releasing pharmacophores.

Acknowledgments

The authors thank Special Project of China (2018ZX0 97201003), NSFC (81673303 and 81703332), BNSF (717 2028), KZ201610025029 and KM201810025010 for financial support.

Disclosure

The authors report no conflicts of interest in this work.

References

1. Aleksandra A, Omar E, Aikaterini E, et al. Molecular and cellular mechanisms of chemoresistance in pancreatic cancer. *Adv Biol Regul*. 2017;68:77–87. doi:10.1016/j.jbior.2017.11.007
2. Ma JL, Hui PP, Meng WY, et al. Ku70 inhibits gemcitabine-induced DNA damage and pancreatic cancer cell apoptosis. *Biochem Biophys Res Commun*. 2017;484:746–752. doi:10.1016/j.bbrc.2017.01.146
3. Lucas DSC, Gisele M. Gemcitabine: metabolism and molecular mechanisms of action, sensitivity and chemoresistance in pancreatic cancer. *Eur J Pharmacol*. 2014;741:8–16. doi:10.1016/j.ejphar.2014.07.041

4. Maria GC, Celine P, Philip WI, et al. Predicting tumour growth and its impact on survival in gemcitabine-treated patients with advanced pancreatic cancer. *Eur J Pharm Sci*. 2018;115:296–303. doi:10.1016/j.ejps.2018.01.033
5. Chi VD. MUC-king with HIF may rewire pyrimidine biosynthesis and curb gemcitabine resistance in pancreatic cancer. *Cancer Cell*. 2017;32:3–5. doi:10.1016/j.ccell.2017.06.006
6. Jia YF, Xie JW. Promising molecular mechanisms responsible for gemcitabine resistance in cancer. *Genes Dis*. 2015;2:299–306. doi:10.1016/j.gendis.2015.07.003
7. Jessica GJ, Carlos M, Pankaj G, et al. Fatal acute cardiac vasculopathy during cisplatin-gemcitabine-bevacizumab (CGB) chemotherapy for advanced urothelial carcinoma. *J Infect Chemother*. 2016;22:112–116. doi:10.1016/j.jiac.2015.08.015
8. Metin U, Manisha K, Ramesh P, et al. Dual delivery nanoscale device for miR-345 and gemcitabine co-delivery to treat pancreatic cancer. *J Control Release*. 2019;294:237–246. doi:10.1016/j.jconrel.2018.12.031
9. Fernando R, Manuel B, Javier G, et al. Tumor treating fields in combination with gemcitabine or gemcitabine plus nab-paclitaxel in pancreatic cancer: results of the PANOVA phase 2 study. *Pancreatology*. 2019;19:64–72.
10. Yeo WK, Ji EL, Kyung HJ, et al. KRAS targeting antibody synergizes anti-cancer activity of gemcitabine against pancreatic cancer. *Cancer Lett*. 2018;348:174–186.
11. Qian WK, Li J, Chen K, et al. Metformin suppresses tumor angiogenesis and enhances the chemosensitivity of gemcitabine in a genetically engineered mouse model of pancreatic cancer. *Life Sci*. 2018;208:253–261. doi:10.1016/j.lfs.2018.07.046
12. Lou CJ, Lu HB, Ma ZG, et al. Ginkgolide B enhances gemcitabine sensitivity in pancreatic cancer cell lines via inhibiting PAFR/NF-κB pathway. *Biomed Pharmacother*. 2019;109:563–572. doi:10.1016/j.biopha.2018.10.084
13. AnnaL S, NP K, Marta G, et al. Melatonin and its metabolite N1-acetyl-N2-formyl-5- methoxykynuramine (afmk) enhance chemosensitivity to gemcitabine in pancreatic carcinoma cells (PANC-1). *Pharmacol Rep*. 2018;70:1079–1088. doi:10.1016/j.pharep.2018.05.007
14. Sunny G, Rahul JS, Ved B, et al. Role of gemcitabine and cisplatin as neoadjuvant chemotherapy in muscle invasive bladder cancer: experience over the last decade. *Asian J Urol*. 2019;6:222–229.
15. Claudio V, Michele P, Monica M, et al. Single-agent gemcitabine vs. carboplatin-gemcitabine in advanced breast cancer: a retrospective comparison of efficacy and safety profiles. *Clin Breast Cancer*. 2019;19:306–318.
16. Michael EH, Paul M, Yao XP, et al. Multicenter phase 2 trial of gemcitabine, carboplatin, and sorafenib in patients with metastatic or unresectable transitional-cell carcinoma. *Clin Genitourin Cancer*. 2018;16:437–444. doi:10.1016/j.clgc.2018.07.021
17. Hayley SM, Graham M, Robert H, et al. Salvage chemotherapy with gemcitabine, paclitaxel, ifosfamide, and cisplatin for relapsed germ cell cancer. *Clin Genitourin Cancer*. 2018;16(6):458–465. doi:10.1016/j.clgc.2018.07.006
18. Hiroki F, Hiroshi K, Hisashi K, et al. Successful treatment with paclitaxel, carboplatin, and gemcitabine as second-line chemotherapy for recurrent urothelial carcinoma of the bladder with glandular differentiation after radical cystectomy: a case report. *Urol Case Rep*. 2017;15:11–13. doi:10.1016/j.eucr.2017.08.001
19. Chen HM, Pan CC, Tsai CM, et al. Concomitant primary lung cancer and metastatic pulmonary colorectal cancer that responded to gemcitabine/cisplatin/bevacizumab combination therapy. *J Cancer Res Pract*. 2015;2(1):76–82.
20. Agnès D, Sophie C, Nuria K, et al. Gemcitabine-based chemotherapy in sarcomas: a systematic review of published trials. *Crit Rev Oncol Hematol*. 2016;98:73–80. doi:10.1016/j.critrevonc.2015.10.020
21. Wang YF, Wang SL, Liu JH, et al. Licoricidin enhances gemcitabine-induced cytotoxicity in osteosarcoma cells by suppressing the Akt and NF-κB signal pathways. *Chem Biol Interact*. 2018;290:44–51. doi:10.1016/j.cbi.2018.05.007
22. Patrizia G, Gregory RP, Guru S, et al. The impact of adding taxanes to gemcitabine and platinum chemotherapy for the first-line therapy of advanced or metastatic urothelial cancer: a systematic review and meta-analysis. *Eur Assoc Urol*. 2016;69:624–633. doi:10.1016/j.eururo.2015.09.051
23. Yang Y, Zhang LJ, Bai XG, et al. Synergistic antitumour effects of triptolide plus gemcitabine in bladder cancer. *Biomed Pharmacother*. 2018;106:1307–1316. doi:10.1016/j.biopha.2018.07.083
24. Fan ML, Liang XF, Li ZH, et al. Chlorambucil gemcitabine conjugate nanomedicine for cancer therapy. *Eur J Pharm Sci*. 2015;79:20–26. doi:10.1016/j.ejps.2015.08.013
25. Sun M, Zhao WY, Xie QP, et al. Lentinan reduces tumor progression by enhancing gemcitabine chemotherapy in urothelial bladder cancer. *Surg Oncol*. 2015;24:28–34. doi:10.1016/j.suronc.2014.11.002
26. Yang CG, Song WT, Zhang SW, et al. Poly (L-glutamic acid)-g-methoxy poly (ethylene glycol)-gemcitabine conjugate improves the anticancer efficacy of gemcitabine. *Int J Pharm*. 2018;550:79–88. doi:10.1016/j.ijpharm.2018.08.037
27. Lionel S, Laurent M, Paul M, et al. Gemcitabine-induced myopathy. *Semin Arthritis Rheum*. 2014;43:784–791. doi:10.1016/j.semarthrit.2013.11.009
28. Amit M, Jonathan SL. Gemcitabine-associated acute lipodermatosclerosislike eruption: an underrecognized phenomenon. *JAAD Case Reports*. 2017;3(3):190–195. doi:10.1016/j.jdcr.2017.02.014
29. Tahir EY, Sibel IT, Sevgi T. Development and characterization of gemcitabine hydrochloride loaded lipid polymer hybrid nanoparticles (LPHNs) using central composite design. *Int J Pharm*. 2018;548:255–262. doi:10.1016/j.ijpharm.2018.06.063
30. Carlotta B, Fransisca L, Yeonju L, et al. Gemcitabine enhances the transport of nanovector- albumin-bound paclitaxel in gemcitabine-resistant pancreatic ductal adenocarcinoma. *Cancer Lett*. 2017;403:296–304. doi:10.1016/j.canlet.2017.06.026
31. Nuno V, Abigail F, Iva F, et al. Gemcitabine anti-proliferative activity significantly enhanced upon conjugation with cell-penetrating peptides. *Bioorg Med Chem Lett*. 2017;27:2898–2901. doi:10.1016/j.bmcl.2017.04.086
32. Gebremariam B, Hamid A, Ehsan S, et al. Nanotechnology for delivery of gemcitabine to treat pancreatic cancer. *Biomed Pharmacother*. 2017;88:635–643. doi:10.1016/j.biopha.2017.01.071
33. Zhou Y, Chang QQ, Wang WJ, et al. Sensitive analysis and pharmacokinetic study of a novel gemcitabine carbamate prodrug and its active metabolite gemcitabine in rats using LC-ESI-MS/MS. *J Chromatogr B*. 2018;1083:249–257. doi:10.1016/j.jchromb.2018.03.015
34. Ravindra DD, Ankit S, Prasoon K, et al. Recent advances in drug delivery strategies for improved therapeutic efficacy of gemcitabine. *Eur J Pharm Sci*. 2016;93:147–162. doi:10.1016/j.ejps.2016.08.021
35. Wang ZM, Chen LN, Chu ZY, et al. Gemcitabine-loaded gold nanospheres mediated by albumin for enhanced anti-tumor activity combining with CT imaging. *Mater Sci Eng C*. 2018;89:106–118. doi:10.1016/j.msec.2018.03.025
36. Arnaud P, Simona M, Semen OY, et al. Squalene versus cholesterol: which is the best nanocarrier for the delivery to cells of the anticancer drug gemcitabine? *C R Chim*. 2018;21:974–986. doi:10.1016/j.crci.2018.02.008
37. Ma L, Chen YC, Wang XD, et al. Design, characterization, and in vitro antiproliferative efficacy of gemcitabine conjugates based on carboxymethyl glucan. *Bioorg Med Chem Lett*. 2018;28:2920–2924. doi:10.1016/j.bmcl.2018.07.014
38. Yuan Z, Xin B, Bingfang Y, et al. Gemcitabine nanoparticles promote antitumor immunity against melanoma. *Biomaterials*. 2019;189:48–59. doi:10.1016/j.biomaterials.2018.10.022

39. Jun YP, Ye LC, Ju RC, et al. Gemcitabine-incorporated G-quadruplex aptamer for targeted drug delivery into pancreas cancer. *Mol Ther*. 2018;12:543–553. doi:10.1016/j.omtn.2018.06.003
40. Jansen WJM, Pinedo HM, Wilt CLVD, et al. The influence of BIBW22BS, a dipyridamole derivative, on the antiproliferative effects of 5-fluorouracil, methotrexate and gemcitabine in vitro and in human tumour xenografts. *Eur J Cancer*. 1995;31(13):2313–2319. doi:10.1016/0959-8049(95)00440-8
41. Andries MB, Herbert MP, Godefridus JP. Determinants of resistance to 2',2'-difluorodeoxycytidine (gemcitabine). *Drug Resist Updat*. 2002;5:19–33.
42. Vaibhav K, Smit K, Noor A, et al. Synthesis, characterization and mechanistic-insight into the anti-proliferative potential of PLGA-gemcitabine conjugate. *Int J Pharm*. 2014;470:51–62. doi:10.1016/j.ijpharm.2014.05.005
43. Jin SM, Wang YN, Zhu HM, et al. Nanosized aspirin-Arg-Gly-Asp-Val: delivery of aspirin to thrombus by the target carrier Arg-Gly-Asp-Val tetrapeptide. *ACS Nano*. 2013;7(9):7664–7673. doi:10.1021/nn402171v
44. Yu HL, Mei SH, Zhao M, et al. RGD-peptides modifying dexamethasone: to enhance the anti-inflammatory efficacy and limit the risk of osteoporosis. *Med Chem Comm*. 2015;6:1345–1351. doi:10.1039/C5MD00215J
45. Wu JH, Zhu HM, Zhao M, et al. IQCA-TASS: a nano-scaled P-selectin inhibitor capable of targeting thrombus and releasing IQCA/TARGD(S)S in vivo. *J Mater Chem B*. 2017;5:917–927. doi:10.1039/C6TB02705A
46. P J L, Charles D. Review of recent studies on resistance to cytotoxic deoxynucleoside analogues. *Biochim Biophys Acta*. 2007;1776:138–159. doi:10.1016/j.bbcan.2007.07.004